



1 GROWTH OF A SINKHOLE IN A SEISMIC ZONE OF THE NORTHERN APENNINES (ITALY)  
2 Alessandro La Rosa<sup>1,2</sup>, Carolina Pagli<sup>2</sup>, Giancarlo Molli<sup>2</sup>, Francesco Casu<sup>3</sup>, Claudio De Luca<sup>3</sup>,  
3 Amerino Pieroni<sup>4</sup>

4  
5 <sup>1</sup> Dipartimento di Scienze della Terra, Università degli Studi di Firenze, Via G. La Pira, 4, 50121 Firenze, Italy  
6 <sup>2</sup> Dipartimento di Scienze della Terra, Università di Pisa, Via S. Maria, 53, 56126 Pisa, Italy  
7 <sup>3</sup> CNR, Consiglio Nazionale delle Ricerche, Istituto per il Rilevamento Elettromagnetico dell'Ambiente (IREA-  
8 CNR), Via Diocleziano, 328, 80124 Napoli, Italy  
9 <sup>4</sup> Pro.Geo. s.r.l. Via Valmaira, 14, 55032, Castelnuovo di Garfagnana, Italy

10

11 **Keywords:** Sinkhole, InSAR, Seismicity

## 12 **Abstract**

13 Sinkhole collapse is a major hazard causing substantial social and economic losses. However,  
14 the surface deformations and sinkhole evolution are rarely recorded, as these sites are known  
15 mainly after a collapse, making the assessment of sinkholes-related hazard challenging.  
16 Furthermore, 40% of the sinkholes of Italy are in seismically hazardous zones; it remains unclear  
17 whether seismicity may trigger sinkhole collapse. Here we use a multidisciplinary dataset of InSAR,  
18 surface mapping and historical records of sinkhole activity to show that the Prà di Lama lake is a  
19 long-lived sinkhole that was formed over a century ago and grew through several events of unrest  
20 characterized by episodic subsidence and lake-level changes. Moreover, InSAR shows that  
21 continuous aseismic subsidence at rates of up to 7.1 mm yr<sup>-1</sup> occurred during 2001-2008, between  
22 events of unrest. Earthquakes on the major faults near the sinkhole are not a trigger to sinkhole  
23 activity but small-magnitude earthquakes at 4-12 km depth occurred during sinkhole unrest in  
24 1996 and 2016. We interpret our observations as evidence of seismic creep in an active fault zone  
25 at depth causing fracturing and ultimately leading to the formation and growth of the Prà di Lama  
26 sinkhole.

27



28        **1. Introduction**

29            Sinkholes are quasi-circular depressions in the ground surface that form due to the  
30 breakdown of subterranean cavities (*Neuendorf et al., 2005*). Sinkhole subsidence and collapse  
31 cause substantial economic and human losses globally (*Frumkin and Raz, 2001; Wadas, 2017;*  
32 *Closson, 2005*). In Italy, a total of 750 sinkholes have been identified by *Caramanna et al. (2008)*.

33            Typically, sinkholes form in karst landscapes where the exposed soluble rocks are dissolved  
34 by circulating ground water (dissolution sinkholes) but deep sinkholes also develop by  
35 erosion/dissolution of a deep layer of rock covered by non-soluble rocks (*Caramanna et al., 2008*).  
36 In particular, deep sinkholes have been observed along seismically active faults indicating a causal  
37 link between sinkhole formation and active tectonics (*Faccenna et al., 1993; Closson et al., 2005;*  
38 *Florea, 2005; Harrison et al., 2002; Wadas et al., 2017*). The processes responsible for the  
39 formation of these sinkholes have been attributed to fracturing and increased permeability in the  
40 fault damage zone promoting fluid circulation and weathering of soluble rocks at depth.  
41 Additionally, when carbonate bedrocks lie below thick non-carbonate formations, stress changes  
42 caused by faulting may cause decompression of confined aquifers favouring upward migration of  
43 deep acid fluids hence promoting erosion and collapses; a process known as Deep Piping  
44 (*Caramanna et al., 2008*). Sinkhole formation can also be triggered by faulting and two sinkholes  
45 formed near En Gedi, Dead Sea, following the  $M_w$  5.2 earthquake on the Dead Sea Transform Fault  
46 in 2004 (*Salamon, 2004*).

47            The sinkhole of Prà di Lama, near the Pieve Fosciana town (Lucca, Italy), is a circular  
48 depression filled by a lake (*Caramanna et al., 2008*). Prà di Lama is located in the seismically active  
49 Apennine range of Northern Tuscany, at the intersection between two active faults (Fig. 1). Hot  
50 springs are also present at Pieve Fosciana suggesting that fluid migration along the faults planes



51 occurs. Sudden lake-level changes of up to several meters, ground subsidence, surface fracturing  
52 and seismicity have occurred repeatedly since at least 991 A.D. (*Nisio, 2008*). The most recent  
53 deformation events occurred in March 1996 and between May 2016 and October 2017. However,  
54 the processes that control the growth of the Prà di Lama sinkhole remain unclear. Furthermore,  
55 whether seismicity along the active faults around Pra di Lama may trigger sinkhole subsidence or  
56 collapse is debated.

57 In this paper we combine recent InSAR observations, seismicity, and surface mapping, as  
58 well as historical records of lake-level changes and ground subsidence at the Prà di Lama from  
59 1828 to understand the mechanisms of sinkhole growth in an active fault system.

## 60 **2. Geological Background**

61 The area of the Prà di Lama sinkhole is located within the Garfagnana basin (Fig.1), an  
62 extensional graben in the western Northern Apennines, a NW-SE trending fold-and-thrust belt  
63 formed by the stack of different tectonic units caused by the convergence of the Corsica-European  
64 and Adria plates. the current tectonic regime of the Apennines is characterized by shortening in  
65 the eastern sector of the Apennine range and extension in the westernmost side of the range  
66 (*Elter et al., 1975; Patacca and Scandone, 1989; Bennett et al., 2012*). The contemporaneous  
67 eastward migration of shortening and upper plate extension are believed to be caused by the roll-  
68 back subduction during the counter-clockwise rotation of the Adria plate (*Dogliani, 1991; Meletti*  
69 *et al., 2000; Serpelloni et al., 2005; Faccenna et al., 2014; Le Breton et al., 2017 and references*).  
70 Extension started 4-5 Ma ago leading to the formation of several NW-SE-oriented grabens,  
71 bounded by NE-dipping and SW-dipping normal faults that are dissected by several NE-trending,  
72 right-lateral strike-slip faults (Fig. 1). The inner northern Apennines are a seismically active area,  
73 where several earthquakes with  $M_w > 5$  occurred, including the largest instrumentally recorded  
74 earthquake,  $M_w$  6.5, in 1920 (*Tertulliani and Maramai, 1998; Rovida et al., 2016; Bonini et al.,*



75 2016) and the most recent  $M_w$  5.1 earthquake in 2013 (Pezzo *et al.*, 2014; Stramondo *et al.*, 2014;  
76 Molli *et al.*, 2016).

77 The uppermost stratigraphy of the Prà di Lama sinkhole consists of an eight-meters-thick  
78 layer of alluvial and palustrine gravels and sandy deposits containing pity levels, covering ~60-m-  
79 thick sandy-to-silty fluvio-lacustrine deposits with low permeability (from Villafranchian to present  
80 age) (Chetoni, 1995). These recent deposits cover a turbiditic sequence named Macigno Fm. Below  
81 the Macigno Fm. a sequence of carbonate rocks pertaining to the Tuscan Nappe Unit is present.  
82 The Prà di Lama sinkhole is located at the intersection between two seismically active faults: the  
83 Corfino normal fault (Di Naccio *et al.*, 2013; Itacha working group, 2003; ISIDe working group,  
84 2016) and the right-lateral strike-slip fault M.Perpoli-T.Scoltenna that recently generated the  $M_w$   
85 4.8 earthquake in January 2013 (Fig.1) (Vannoli, 2013; Pinelli, 2013; Molli *et al.*, 2017). Hot water  
86 springs are also present at Prà di Lama and some of them have a water temperature of ~40 °C  
87 [32]. Prà di Lama was classified as a Deep Piping Sinkhole (DPS) as it is a circular depression that  
88 formed on thick impermeable sediments in a fracture zone, likely due to erosion of soluble rocks  
89 at depth (Caramanna *et al.*, 2008). Hot springs are also a common feature of DPSs due to the  
90 presence of pressurized aquifers together with a system of fractures favouring fluid circulation.

### 91 **3. Data**

92 Century-scale historical records of sinkhole activity are available at Prà di Lama and allow us  
93 to determine the timescale of sinkhole evolution as well as to characterize the different events of  
94 unrest, in particular the two most recent events in 1996 and 2016. InSAR time-series analysis is  
95 also carried out to measure ground deformations in the Prà di Lama sinkhole in the time period  
96 between events of unrest. Finally, the local catalogue of seismicity (ISIDE catalogue, INGV) is used  
97 to inform us on the timing and types of brittle failures in the area of the sinkhole.

98



99 **3.1 Historical Record**

100 The first historical record of the Prà di Lama sinkhole dates back to the 991 A.D., when the  
101 area was described as a seasonal shallow pool fed by springs. Since then, the depression grew and  
102 several events of unrest consisting of fracturing and fluctuations of the lake level were reported  
103 (*Raffaelli, 1869; De Stefani, 1879, Giovannetti, 1975*) (Table 1). In Particular, eight events of unrest  
104 were reported, giving an average of 1 event of unrest every 26 years. We conducted direct  
105 observation of surface deformation around the lake for the two most recent events in 1996 and  
106 2016.

107 In 1996, the lake level experienced a fall of up to 4 m (Fig. 2) and at the same time the  
108 springs outside the lake suddenly increase the water outflow. Clay and mud were also ejected by  
109 the springs outside the lake while fractures and slumps occurred within the lake due to the water  
110 drop (Fig. 2). The unrest lasted approximately 2 months, from March to April 1996. During the final  
111 stages, the water level in the lake rose rapidly recovering its initial level and contemporaneously  
112 the springs water flow reduced.

113 In June 2016, an event of unrest consisting of ground subsidence on the western and southern  
114 sides of the Prà di Lama lake started and lasted approximately 9 months, until February 2017.  
115 During this period fractures formed and progressively grew, increasing their throw to up to 70 cm  
116 and affecting a large area on the western side of the lake (Fig. 2). Subsidence around the lake  
117 resulted in an increase of the lake surface in particular on the western side and formation of  
118 tensile fractures (Fig. 2). Unlike the 1996 events of unrest, no lake level changes or increase of  
119 water flow from the springs around the lake were observed.

120  
121  
122  
123



### 124 **3.2 InSAR**

125 InSAR is ideally suited to monitor localized ground deformation such as caused by sinkholes  
126 as it can observe rapidly evolving deformation of the ground at high spatial resolution (*Baer et al.,*  
127 *2002; Castañeda et al., 2009; Abelson et al., 2017; Atzori et al., 2015*). Furthermore, the availability  
128 of relatively long datasets of SAR images in the Apennine allows us to study the behaviour of the  
129 Prà di Lama sinkhole using multi-temporal techniques. We processed a total of 200 interferograms  
130 using SAR images acquired by the ENVISAT satellite between 2003 to 2010 from two distinct tracks  
131 in Ascending or Descending viewing geometry (tracks 215 and 437). We used the Small BAseline  
132 Subset (SBAS) multi-interferogram method originally developed by *Berardino et al. (2002)* and  
133 recently implemented for parallel computing processing (P-SBAS) by *Casu et al. (2014)* to obtain  
134 incremental and cumulative time-series of InSAR Line-of-Sight (LOS) displacements as well as maps  
135 of average LOS velocity. In particular, the InSAR processing has been carried out via the ESA  
136 platform P-SBAS open-access on-line tool named G-POD (Grid Processing On Demand) that allows  
137 generating ground displacement time series from a set of SAR data (*De Luca et al., 2015*).

138 The P-SBAS G-POD tool allows the user to set some key parameters to tune the InSAR  
139 processing. In this work, we set a maximum perpendicular baseline (spatial baseline) of 400 m and  
140 maximum temporal baseline of 1500 days. The geocoded pixel dimension was set to ~80 m by 80  
141 m (corresponding to averaging together 20 pixels in range and 4 pixels in azimuth). We also set a  
142 coherence threshold to 0.8 (0 to 1 for low to high coherence) in order to select only highly  
143 coherent pixels in our interferograms. Excluding poorly coherent pixels reduces the noise in our  
144 final velocity maps and time-series (*De Luca et al., 2015*). We also inspected the series of  
145 interferograms and excluded individual interferograms with low coherence. We identified and  
146 discarded 29 noisy interferograms in track 215A and other 11 interferograms in track 437D. Finally,  
147 we applied an Atmospheric Phase Screen (APS) filtering to mitigate further atmospheric



148 disturbances (*Hassen, 2001*). Accordingly, we used a triangular temporal filter with a width of 400  
149 days to minimize temporal variations shorter than about a year as we focus on steady  
150 deformations rather than seasonal changes. Shorter time interval of 300 days was also tested but  
151 provided more noisy time-series.

152 As a further post processing step (not yet available via the G-POD tool) we also calculated the  
153 vertical and east-west components of the velocity field in the area covered by both the ascending  
154 and descending tracks and assuming no north-south displacement. Given that the study area is  
155 imaged by the ENVISAT satellite from two symmetrical geometries with similar incidence angles  
156 (few degrees of difference), the vertical and east-west components of the velocity field can simply  
157 be obtained solving the following system of equations (*Manzo et al., 2006*):

$$158 \quad \begin{cases} v_H = \frac{\cos \vartheta}{\sin(2\vartheta)} (v_{DESC} - v_{ASC}) = \frac{v_{DESC} - v_{ASC}}{2 \sin \vartheta} \\ v_V = \frac{\sin \vartheta}{\sin(2\vartheta)} (v_{DESC} + v_{ASC}) = \frac{v_{DESC} + v_{ASC}}{2 \cos \vartheta} \end{cases}$$

159 where  $v_H$  and  $v_V$  are the horizontal and vertical component of the velocity field,  $v_{DESC}$  and  $v_{ASC}$   
160 are the average LOS velocities in the Descending and Ascending tracks, respectively;  $\vartheta$  is the  
161 incidence angle.

162 The InSAR P-SBAS analysis shows that significant surface deformation occurs at Pieve  
163 Fosciana between 2003 and 2010. The observed deformation pattern consists of range increase  
164 mainly on the western flank of the Prà di Lama lake. The range increase is observed in both  
165 ascending and descending velocity maps (Fig. 3a, b), with average LOS velocities of up to  $-7.1 \text{ mm}$   
166  $\text{yr}^{-1}$  decaying to  $-1 \text{ mm yr}^{-1}$  over a distance of 400 m away from the lake. Elsewhere around the lake  
167 coherence is not kept due to ground vegetation cover but few coherent pixels on eastern flank of  
168 the lake suggest that the deformation pattern may be circular, with a radius of  $\sim 600 \text{ m}$  (Fig. 3e).  
169 The maps of vertical and East-West velocities show vertical rates of  $-4.6 \text{ mm yr}^{-1}$  and horizontal



170 eastward velocities of  $5.4 \text{ mm yr}^{-1}$  (Fig. 3c, d) consistent with subsidence and contraction centred  
171 at the lake. Furthermore, figure 4 shows that the current deformation pattern follows the  
172 topography, suggesting that subsidence at Prà di Lama is a long-term feature. The time-series of  
173 cumulative LOS displacements show that subsidence occurred at an approximately constant rate  
174 between the 2003 and the 2008 but it slowed down in 2008 (Fig. 3e, f), indicating that subsidence  
175 at Prà di Lama occurs also between events of unrest. Furthermore, our time-series of vertical and  
176 east-west cumulative displacements also confirm that the fastest subsidence and  
177 contemporaneous eastward motion occurred until 2008 (Fig. 3g, h). In order to better understand  
178 the mechanisms responsible for the sinkhole growth and the different types of episodic unrest we  
179 also analysed the seismicity.

### 180 3.3 Seismicity

181 We analysed the seismicity at the Prà di Lama lake using the catalogue ISIDe (Italian  
182 Seismological Instrumental and Parametric Data-Base) spanning the time period from 1986 to  
183 2016. We calculated the cumulative seismic moment release using the relation between seismic  
184 moment and magnitudes given by *Kanamori (1977)*. First, we analysed the seismic moment  
185 release and the magnitude content of the earthquakes in the area encompassing the sinkhole and  
186 the faults intersection (10 km radius, Fig. 1) to understand whether unrest at Prà di Lama is  
187 triggered by earthquakes along the active faults (Fig. 5). Fig. 4a shows that although several  
188 seismic swarms occurred in the area, no clear temporal correlation between the swarms and the  
189 events of unrest at Prà di Lama is observed, suggesting that the majority of seismic strain released  
190 on faults around the Prà di Lama lake does not affect the activity of the sinkhole. We removed  
191 from the plot in Fig. 4a the large magnitude earthquake,  $M_w$  4.8, on the 25<sup>th</sup> of January 25, 2013 in  
192 order to better visualize the pattern of seismic moment release in time. In any case, no activity at  
193 Prà di Lama was reported in January 2013.





194 We also analysed the local seismicity around the Prà di lama lake, within a circular area of 3  
195 km radius around the lake (Fig. 1), to better understand the deformation processes occurring at  
196 the sinkhole (Fig. 6) and we found that swarms of small-magnitude earthquakes ( $M_L \leq 2$ ) occurred  
197 during both events of unrest at Prà di Lama in 1996 and 2016 (Fig. 6a, b, c), while a few  
198 earthquakes with magnitudes  $> 2$  occurred irrespective of the events of unrest. This indicates that  
199 seismicity during sinkhole activity is characterized by seismic energy released preferentially  
200 towards the small end of magnitudes spectrum. This pattern is specific of the sinkhole area as in  
201 the broader region (Fig. 5b, c) the majority of earthquakes magnitudes are in the range between  
202  $M_L > 2$  and  $M_L < 3$  and few  $M_L > 3$  also occurred. We also analysed the hypocentres of the  
203 earthquakes around the Prà di lama lake (3 km radius) and find that these range between 4.5 and  
204 11.5 km depth, indicating that deformation processes in the fault zone control the sinkhole  
205 activity. On the other hand, no earthquakes were recorded at Prà di Lama during the period of  
206 subsidence identified by InSAR between 2003 and 2010, indicating that subsidence between  
207 events of unrest continuous largely aseismically.

#### 208 4. Discussion and conclusions

209 A multi-disciplinary dataset of InSAR measurements, field observations and seismicity reveal  
210 that diverse deformation events occur at the Prà di Lama sinkhole. Two main events of sinkhole  
211 unrest occurred at Prà di Lama in 1996 and 2016 but the processes had different features. In 1996  
212 the lake-level dropped together with increased water outflow from the springs, while in 2016  
213 ground subsidence led to the expansion of the lake surface and fracturing. Furthermore, InSAR  
214 analysis shows that continuous but aseismic subsidence of the sinkhole occurred between the two  
215 events of unrest, during the period 2003-2010. Instead swarms of small-magnitude earthquakes  
216 coeval to the unrest events of 1996 and 2016 were recorded at depth between 4.5 and 11.5 km,



217 indicating that a link between seismicity and sinkhole activity exists. We suggest that seismic creep  
218 in the fault zone underneath Prà di Lama occurs, causing the diverse deformation events. Seismic  
219 creep at depth could have induced pressure changes in the aquifer above the fault zone (1996  
220 events) as well as causing subsidence by increased fracturing (2016 events). The seismicity pattern  
221 revealed by our analysis suggests that the Mt.Perpoli-T.Scoltenna strike-slip fault system  
222 underneath Prà di Lama is locally creeping, producing seismic sequences of low magnitude  
223 earthquakes. Similar seismicity patterns were observed in 2006 along the Superstition Hills fault  
224 (San Andreas fault system, California) where seismic creep is favoured by high water pressure (*Wei*  
225 *et al., 2009; Scholz, 1998; Harris, 2017*). We suggest that at the Prà di Lama fault zone an increase  
226 in pressure in the aquifer in 1996 caused fracturing at the bottom of the lake and upward  
227 migration of fluids rich in clays, in agreement with the observations of lake-level drop and mud-  
228 rich water ejected by the springs in 1996. Sudden fracturing and periods of compaction of cavities  
229 created by enhanced rock dissolution in the fluid circulation zone also explains both sudden  
230 subsidence and fracturing, as in 2016, and periods of continuous but aseismic subsidence as in  
231 2003-2010. Similar processes have been envisaged for the formation of a sinkhole at the  
232 Napoleonville Salt Dome, where a seismicity study suggests that fracturing enhanced the rock  
233 permeability, promoting the rising of fluids and, as a consequence, erosion and creation of deep  
234 cavities prone to collapse (*Yarushina et al., 2017; Sibson, 1996; Micklethwaite et al., 2010, Nayak*  
235 *and Dreger, 2014*). Recently, a sequence of seismic events was identified at Mineral Beach (Dead  
236 Sea fault zone) and was interpreted as the result of cracks formation and faulting above  
237 subsurface cavities (*Abelson et al., 2017*).

238 Precursory subsidence of years to few months has been observed to precede sinkhole  
239 collapse in carbonate or evaporitic bedrocks (e.g. *Baer et al., 2002; Nof et al., 2013; Cathleen and*  
240 *Bloom, 2014; Atzori et al., 2015; Abelson et al., 2017*). However, the timing of these processes



241 strongly depends on the rheological properties of the rocks (*Shalev and Lyakhovsky, 2013*).  
242 Furthermore, the presence of a thick lithoid sequence in Prà di Lama could mean that the sinkhole  
243 will not collapse into the underlying cavities, also in agreement with the exceptionally long  
244 timescale (~200 years) of growth of the Prà di Lama sinkhole (*Caramanna et al., 2008; Shalev*  
245 *and Lykovsky, 2012; Abelson et al., 2017*). However, at present we are not able to establish if and  
246 when a major collapse will occur in Prà di Lama.

247 We identified a wide range of surface deformation patterns associated with the Prà di Lama  
248 sinkhole and we conclude that a source mechanism for the sinkhole formation and growth is  
249 seismic creep in the active fault zone underneath the sinkhole. This mechanism could control the  
250 evolution of other active DPSs in Italy as well as in other areas worldwide where sinkhole form in  
251 active fault systems (e.g. Dead Sea area). InSAR monitoring has already shown to be a valid  
252 method to detect precursory subsidence occurring before a sinkhole collapse and the recent SAR  
253 missions, such as the European Sentinel-1, will very likely provide a powerful tool to identify such  
254 deformations.

255

256

257

258

259

260

261

262



263 **References**

264

265 Abelson, M., Aksinenko, T., Kurzon, I., Pinsky, V., Baer, G., Nof, R., & Yechieli, Y.: Nanoseismicity forecast  
266 sinkhole collapse in the Dead Sea coast years in advance. <https://doi.org/10.1130/G39579.1> (2017)

267 Atzori, S., Baer, G., Antonioli, A., & Salvi, S.: InSAR-based modelling and analysis of sinkholes along the Dead  
268 Sea coastline. *Geophysical Research Letters*, 42, 8383–8390. <https://doi.org/10.1002/2015GL066053>  
269 (2015)

270 Bencini, A., Duchi, V., Martini, M.: Geochemistry of thermal springs of Tuscany (Italy). *Chemical Geology*, 19,  
271 229-252. (1977)

272 Baer, G., Schattner, U., Wachs D., Sandwell, D., Wdowinski, S., Frydman, S.: The lowest place on Earth is  
273 subsiding – An InSAR (Interferometric Synthetic Aperture Radar) Perspective. *Geological Society of  
274 America Bulletin*, 114 (1), 12-23. [https://doi.org/10.1130/00167606\(2002\)114<0012:TLPOEI>2.0.CO;2](https://doi.org/10.1130/00167606(2002)114<0012:TLPOEI>2.0.CO;2)  
275 (2002)

276 Bennet, R.A., Serpelloni, E., Hreinsdottir, S., Brandon, M.T., Buble, G., Basic T., Casale, G., Cavaliere, A.,  
277 Anzidei, M., Marjonovic, Minelli, G., Molli, G., & Montanari, A.: Syn-convergent extension observed  
278 using the RETREAT GPS network, northern Apennines, Italy. *Journal of Geophysical Research*, 117.  
279 <https://doi.org/10.1029/2011JB008744> (2012)

280 Berardino, P., Fornaro, G., Lanari, R., & Sansosti, E.: A new algorithm for surface deformation monitoring  
281 based on Small Baseline Differential SAR interferograms. *IEEE International Geoscience and Remote  
282 Sensing Symposium*, 40(11). <https://doi.org/10.1109/TGRS.2002.803792> (2002)

283 Bonini, M., Corti, G., Donne, D. D., Sani, F., Piccardi, L., Vannucci, G., Genco, R., Martelli, L., Ripepe, M.:  
284 Seismic sources and stress transfer interaction among axial normal faults and external thrust fronts in  
285 the northern Apennines (Italy): a working hypothesis based on the 1916-1920 time-space cluster of  
286 earthquakes. *Tectonophysics*, 680, 67–89. <https://doi.org/10.1016/j.tecto.2016.04.045> (2016)

287 Caramanna, G., Ciotoli, G., Nisio, S.: A review of natural sinkhole phenomena in Italian plain areas. *Natural  
288 Hazards*, 45, 145–172. <https://doi.org/10.1007/s11069-007-9165-7> (2008)

289 Castañeda, C., Gutiérrez, F., Manunta, M., Galve, J. P.: DInSAR measurements of ground deformation by  
290 sinkholes, mining subsidence, and landslides, Ebro River, Spain. *Earth Surf. Process. Landforms*, 34, 11,  
291 1562–1574. <https://doi.org/10.1002/esp.1848> (2009)

292 Casu, F., Elefante, S., Imperatore, P., Zinno, I., Manunta, M., De Luca, C., & Lanari, R: SBAS-DInSAR parallel  
293 processing for deformation time-series computation. *IEEE Journal of Selected Topics in Applied Earth  
294 Observations and Remote Sensing*, 7(8), 3285–3296. <https://doi.org/10.1109/JSTARS.2014.2322671>.  
295 (2014)

296 Cathleen, J., & Blom, R.: Bayou Corne, Louisiana, sinkhole: Precursory deformation measured by radar  
297 interferometry. *Geology*. 42 (2), 111-114. <https://doi.org/10.1130/G34972.1> (2014)

298 Chetoni, R.: Terme di Prà di Lama (Pieve Fosciana, Lu), indagine geognostica sulle aree dissestate nel marzo  
299 1996. Geological Report. (1996)



- 300 Closson, D.: Structural control of sinkholes and subsidence hazards along the Jordanian Dead Sea coast.  
301 *Environmental Geology*, 47 (2), 290-301. <https://doi.org/10.1007/s00254-004-1155-4> (2005)
- 302 Closson, D., Karaki, N.A., Klinger, Y., & Hussein, M. J.: Subsidence and Sinkhole Hazard Assessment in the  
303 Southern Dead Sea Area, Jordan. *Pure and Applied Geophysics*, 162, 221–248.  
304 <https://doi.org/10.1007/s00024-004-2598-y> (2005)
- 305 De Luca, C., Cuccu, R., Elefante, S., Zinno, I., Manunta, M., Casola, V., Rivolta, G., Lanari, R., Casu, F.: An On-  
306 Demand Web Tool for the Unsupervised Retrieval of Earth's Surface Deformation from SAR Data: The  
307 P-SBAS Service within the ESA G-POD Environment. *Remote Sensing*, 7(11), 15630-15650.  
308 <https://doi.org/10.3390/rs71115630> (2015)
- 309 De Stefani, C.: Le Acque Termali di Pieve Fosciana. *Memorie della Società Toscana di Scienze Naturali*, 4,  
310 72-97 (1879)
- 311 Di Naccio, D., Boncio, P., Brozzetti, F., Pazzaglia, F. J., & Lavecchia, G.: Morphotectonic analysis of the  
312 Lunigiana and Garfagnana grabens (northern Apennines, Italy): Implications for active normal faulting.  
313 *Geomorphology*, 201, 293–311. <https://doi.org/10.1016/j.geomorph.2013.07.003> (2013)
- 314 Doglioni, C.: A proposal for the kinematic modelling of the W-dipping subduction – possible applications to  
315 the Tyrrhenian-Apennines system. *Terra Nova*, 3, 423-434. <https://doi.org/10.1111/j.1365-3121.1991.tb00172.x> (1991)
- 317 Elter, P., Giglia, G., Tongiorgi, M., Trevisan, L.: Tensional and compressional areas in the recent (Tortonian  
318 to Present) evolution of the Northern Apennines. *Bollettino di Geofisica Teorica ed Applicata*, 65 (8)  
319 (1975)
- 320 Faccenna, C. Florindo, F., Funicello, R., Lombardi, S.: Tectonic setting and Sinkhole Features: case histories  
321 from Western Central Italy. *Quaternary Proceedings*, 3, 47–56 (1993)
- 322 Faccenna, C. Becker, T.W., Miller, S.M., Serpelloni, E., & Willet, S.D.: Isostasy, dynamic topography, and the  
323 elevation of the Apennines of Italy. *Earth and Planetary Science Letters*, 407, 163–174.  
324 <https://doi.org/10.1016/j.epsl.2014.09.027> (1993)
- 325 Florea, L. J.: Using State-wide GIS data to identify the coincidence between sinkholes and geologic structure.  
326 *Journal of Cave and Karst Studies*, (August), 120–124. Retrieved from  
327 [http://digitalcommons.wku.edu/geog\\_fac\\_pub/14](http://digitalcommons.wku.edu/geog_fac_pub/14) (2005)
- 328 Frumkin, A., & Raz, E.: Collapse and subsidence associated with salt karstification along the Dead Sea.  
329 *Carbonates and Evaporites*, 16(2), 117–130. <https://doi.org/https://doi.org/10.1007/bf03175830>  
330 (2001)
- 331 Giovannetti, F.: Pieve Fosciana Ieri e Oggi. (1975)
- 332 Hanssen, R. F.: Radar Interferometry: Data Interpretation and Error Analysis. Kluwer Academic Publisher.  
333 <https://doi.org/10.1007/0-306-47633-9> (2001)
- 334 Harris, R.A.: Large earthquakes and creeping faults. *Reviews of Geophysics*, 55, 169-198.  
335 <https://doi.org/10.1002/2016RG000539> (2017)



- 336 Harrison, R. W., Newell, W. L., & Necdet, M.: Karstification Along an Active Fault Zone in Cyprus. Atlanta,  
337 Georgia. *U.S. Geological Survey Water-Resources Investigations Report 02-4174* (2002)
- 338 ISIDE working group version 1.0 (2016)
- 339 Johnson, A. G., Kovach, R. L., & Nur, A.: Pore pressure changes during creep events on the San Andreas  
340 Fault. *Journal of Geophysical Research*, 78 (5). <https://doi.org/10.1029/JB078i005p00851> (1973)
- 341 Kanamori, H.: The Energy Release in Great Earthquakes. *Journal of Geophysical Research*, 82(20).  
342 <https://doi.org/10.1029/JB082i020p02981> (1977)
- 343 Le Breton, E., Handy, M., Molli, G., & Ustaszewski K.: Post-20 Ma Motion of the Adriatic Plate: New  
344 Constraints from Surrounding Orogens and Implications for Crust-Mantle Decoupling. *Tectonics*, 36.  
345 <https://doi.org/10.1002/2016TC004443> (2000)
- 346 Manzo, M., Ricciardi, G.P., Casu F., Ventura, G., Zeni, G., Borgström S., Berardino, P., Del Gaudio, C., Lanari,  
347 R.: Surface deformation analysis in th Ischia Island (Italy) based on spaceborne radar interferometry.  
348 *Journal of Volcanology and Geothermal Research* 151, 399-416.  
349 <https://doi.org/10.1016/j.jvolgeores.2005.09.010> (2006)
- 350 Meletti, C., Patacca, E., & Scandone P.: Construction of a Seismotectonic Model: The Case of Italy. *Pure and*  
351 *applied Geophysics*, 157, 11-35. <https://doi.org/10.1007/PL00001089> (2000)
- 352 Micklethwaite, S., Sheldon, H. A., & Baker, T.: Active fault and shear processes and their implications for  
353 mineral deposit formation and discovery. *Journal of Structural Geology*, 32(2), 151–165.  
354 <https://doi.org/10.1016/j.jsg.2009.10.009> (2010)
- 355 Molli, G., Torelli, L., & Storti, F.: The 2013 Lunigiana (Central Italy) earthquake: Seismic source analysis from  
356 DInSar and seismological data, and geodynamic implications for the northern Apennines. A discussion.  
357 *Tectonophysics*, 668–669, 108–112. <http://dx.doi.org/10.1016/j.tecto.2015.07.041> (2016)  
358
- 359 Molli, G., Pinelli, G., Bigot, A., Bennett R., Malavieille J., Serpelloni E.: Active Faults in the inner northern  
360 Apennines: a multidisciplinary reappraisal. From 1997 to 2016: Three Destructive Earthquakes along  
361 the Central Apennine Fault system, Italy. July 19<sup>th</sup>-22<sup>nd</sup> 2017 Camerino, Volume Abstract (2017)
- 362 Nayak, A., & Dreger, D. S.: Moment Tensor Inversion of Seismic Events Associated with the Sinkhole at  
363 Napoleonville Salt Dome, Louisiana. *Bulletin of the Seismological Society of America*, 104(4), 1763–  
364 1776. <https://doi.org/10.1785/0120130260> (2014)
- 365 Neuendorf, K., Mehl, J., Jackson, J.: Glossary of geology, 5th edn. *American Geological Institute*, 779 pp.  
366 (2005)
- 367 Nisio, S.: The sinkholes in Tuscany Region. *Memorie Descrittive Carta Geologica d'Italia LXXXV* (2008)
- 368 Nof, R. N., Baer, G., Ziv, A., Raz, E., Atzori, S., & Salvi, S.: Sinkhole precursors along the Dead Sea, Israel,  
369 revealed by SAR interferometry. *Geology*, 41, (9), 1019-1022. <https://doi.org/10.1130/G34505.1>  
370 (2013)
- 371 Patacca, E., & Scandone, P.: Post-Tortonian mountain building in the Apennines, the role of the passive  
372 sinking of a relic lithospheric slab. *The Lithosphere in Italy*, 157–176 (1989).

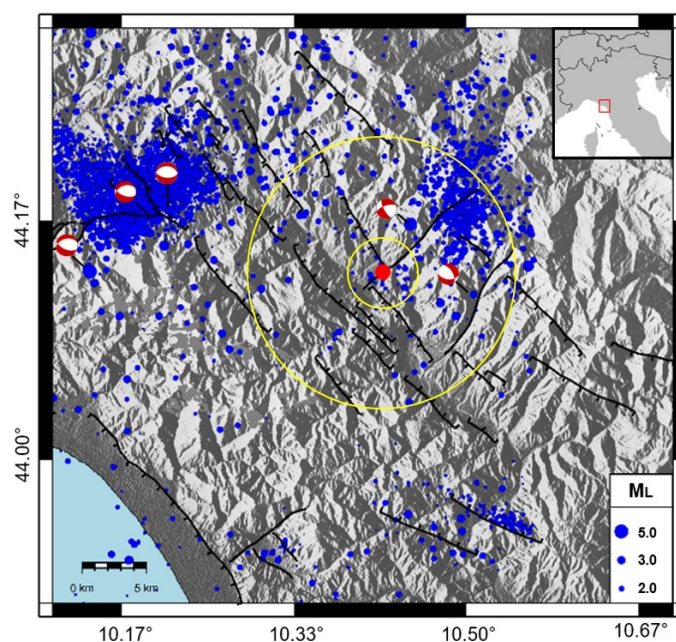


- 373 Pezzo, G., Boncori, J.P.M., Atzori, S., Piccinini, D., Antonioli, A., Salvi, S.: The 2013 Lunigiana (Central Italy)  
374 earthquake: Seismic source analysis from DInSAR and seismological data, and geodynamical  
375 implications for the northern Apennines. *Tectonophysics* 636, 315–324.  
376 <http://dx.doi.org/10.1016/j.tecto.2014.09.005>. (2014)
- 377
- 378 Pinelli, G.: Tettonica recente e attiva nell'Appennino interno a Nord dell'Arno: una revisione delle strutture  
379 e delle problematiche. Diploma Thesis (89 pp) (2013)
- 380 Raffaelli, R.: Sulle acque termali di Pieve Fosciana (1869)
- 381 Rovida A., Locati M., Camassi R., Lolli B., Gasperini P.: CPT15, the 2015 version of the Parametric Catalogue  
382 of Italian Earthquakes. *Istituto Nazionale di Geofisica e Vulcanologia*. [http://doi.org/10.6092/INGV.IT-](http://doi.org/10.6092/INGV.IT-CPT15)  
383 [CPT15](http://doi.org/10.6092/INGV.IT-CPT15) (2016)
- 384 Salamon, A.: Seismically induced ground effects of the February 11, 2004, M L = 5.2, North-eastern Dead  
385 Sea earthquake. *Geological Survey of Israel Report* (2004)
- 386 Serpelloni, E., Anzidei, M., Baldi, P., Casula, G., & Galvani, A.: Crustal velocity and strain -rate fields in Italy  
387 and surrounding regions: New results from the analysis of permanent and non-permanent GPS  
388 networks. *Geophysical Journal International*, 161(3), 861–880.  
389 <https://doi.org/10.1016/j.epsl.2014.03.005> (2005)
- 390 Shalev, E., & Lyakhovsky, V.: Viscoelastic damage modeling of sinkhole formation. *Journal of Structural*  
391 *Geology*, 42, 163–170. <https://doi.org/10.1016/j.jsg.2012.05.010> (2012)
- 392 Scholz, C. H.: Earthquakes and friction laws. *Nature*, 391, 37–42. <https://doi.org/10.1038/34097> (1998)
- 393 Sibson, R. H.: Roughness at the Base of the Seismogenic Zone: Contributing Factors. *Journal of Geophysical*  
394 *Research*, 87 (B7), 5791-5799. <https://doi.org/10.1029/JB089iB07p05791> (1984)
- 395 Sibson, R. H.: Structural permeability of fluid-driven fault-fracture meshes. *Journal of Structural Geology*, 18  
396 (8),1031-1042. [https://doi.org/10.1016/0191-8141\(96\)00032-6](https://doi.org/10.1016/0191-8141(96)00032-6) (1996)
- 397 Stramondo, S., Vannoli, P., Cannelli, V., Polcari, M., Melini, D., Samsonov, S., Moro, M., Bignami, C., & Saroli,  
398 M.: X- and C-band SAR surface displacement for the 2013 Lunigiana earthquake (Northern Italy): a  
399 breached relay ramp? *IEEE J. Sel. Top. Appl. Earth Obs. Remote Sens.*  
400 <http://dx.doi.org/10.1109/JSTARS.2014.2313640> (2014)
- 401 Tertulliani, A., & Maramai, A.: Macroseismic evidence and site effects for the Lunigiana (Italy) 1995  
402 Earthquake. *Journal of Seismology*, 2 (3), 209–222. <https://doi.org/10.1023/A:1009734620985> (1998)
- 403 Vannoli, P.: Il terremoto in Garfagnana del 25 gennaio 2013 visto dal geologo. Retrieved from  
404 [https://ingvterremoti.wordpress.com/2013/02/06/il-terremoto-del-25-gennaio-2013-visto-dal-](https://ingvterremoti.wordpress.com/2013/02/06/il-terremoto-del-25-gennaio-2013-visto-dal-geologo/#more-3132)  
405 [geologo/#more-3132](https://ingvterremoti.wordpress.com/2013/02/06/il-terremoto-del-25-gennaio-2013-visto-dal-geologo/#more-3132) (2013)
- 406 Wadas, S. H., Tanner, D. C., Polom, U., & Krawczyk, C. M.: Structural analysis of S-wave seismics around an  
407 urban sinkhole; evidence of enhanced suberosion in a strike-slip fault zone. *Natural Hazards and Earth*  
408 *System Sciences*. <https://doi.org/10.5194/nhess-2017-315> (2017)



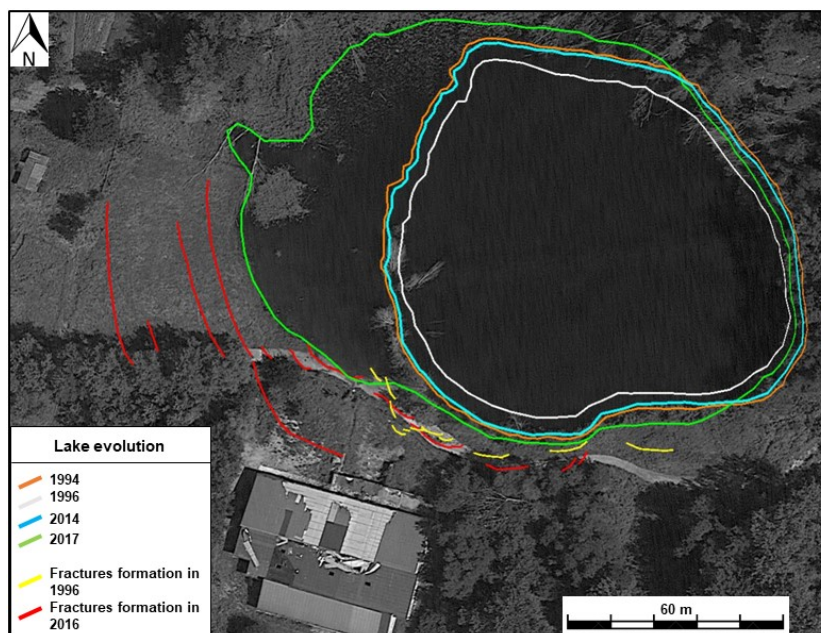


- 409 Wei, M., Sandwell, D., & Fialko, Y.: A silent Mw 4.7 slip event of October 2006 on the Superstition Hills fault,  
410 southern California. *Journal of Geophysical Research*, 114, B07402,  
411 <https://doi.org/10.1029/2008JB006135> (2009)
- 412 Yarushina, V. M., Podladchikov, Y.Y., Minakov, A., & Räss, L.: On the Mechanisms of Stress-Triggered  
413 Seismic Events during Fluid Injection. *Sixth Biot Conference on Poromechanics, American Society of  
414 Civil Engineers*. <https://doi.org/10.1061/9780784480779.098> (2017)



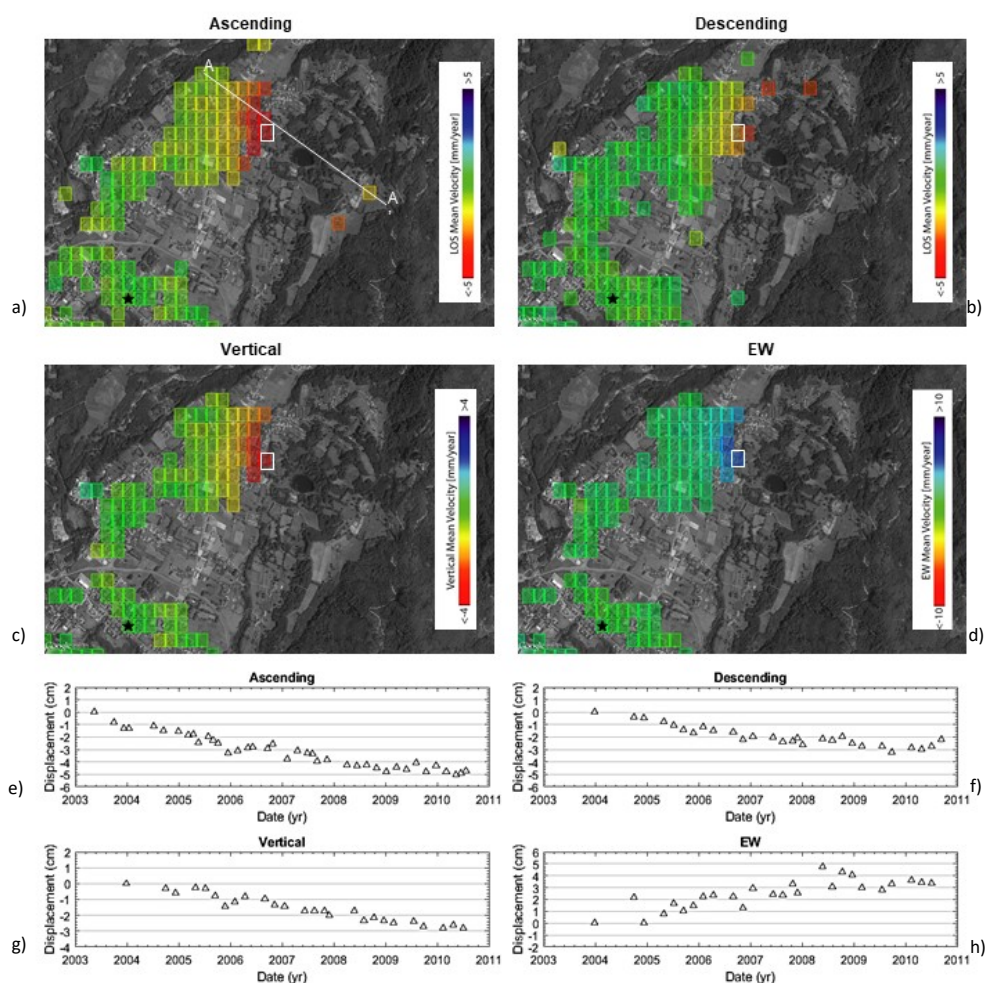
415  
416 **Figure 1 - Study area.** The Pieve Fosciana area is marked by the red dot. Black tick lines are faults. Blue dots are the earthquakes  
417 between 1986 and 2017. Focal mechanisms are from the Regional Centroid Moment Tensor (RCMT) catalogue. The yellow circles  
418 represent the areas with radii of 3km and 10 km used for the seismicity analysis. The red box in the *inset* marks the location of the  
419 area shown in the main figure.





420  
421  
422

**Figure 2 – Evolution of the Prà di Lama lake between 1994 and 2017.** Lake shores variation have been retrieved from the analysis of Landsat image



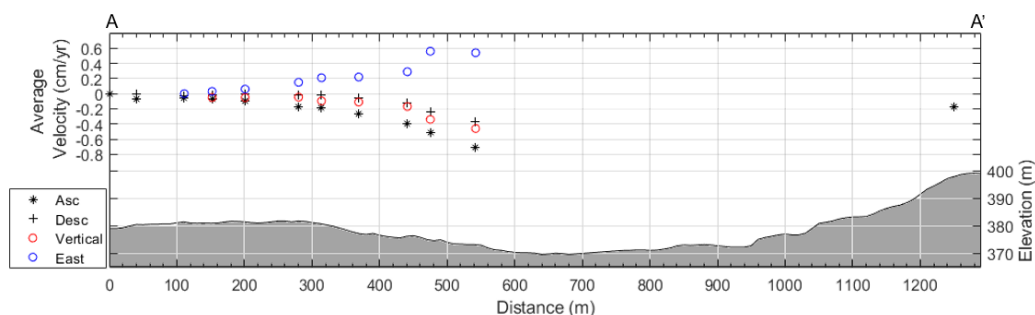
423

424

425

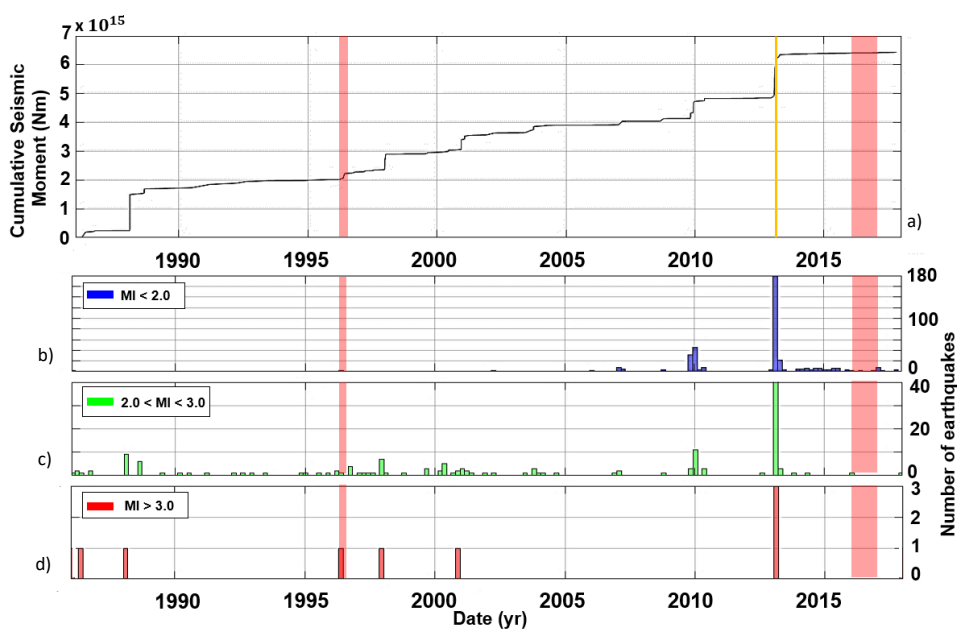
426 **Figure 3 – a, b** Maps of average surface velocity and its vertical (c) and East-West (d) components obtained from ENVISAT SAR  
 427 images acquired between 2003 and 2010. Negative values indicate range increase. The white line in panel a) marks the cross-  
 428 section shown in figure 4. The black star is the point used as reference for the InSAR-SBAS processing. **e, f, g, h** Time-series of  
 429 incremental deformation extracted from the pixel bounded with the white rectangle.

430



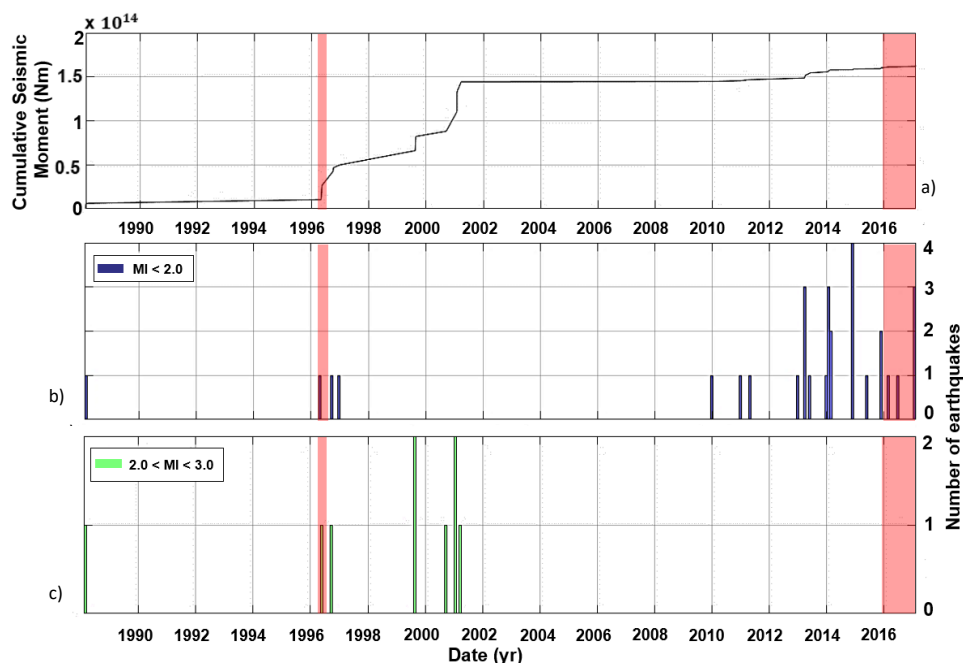
431  
 432 **Figure 4 - Cross-section of topography and InSAR velocities along the A-A' profile as shown in figure 3a.**

433



434  
 435 **Figure 5 – Seismicity within a 10 km radius area around the Prà di Lama lake.** cumulative seismic moment released in the area (a)  
 436 and histograms of the number of earthquakes per month. Three different classes of magnitude have been created: MI < 2.0 (b), 2.0  
 437 < MI < 3.0 (c) and MI > 3.0 (d). The dataset covers the period between 1986 and 2017.

438



439

440 *Figure 6 - Seismicity features of an area 3 km in radius around the Prà di Lama lake.* Plot of the cumulative seismic moment  
 441 released in the area (a) and histograms showing the number of earthquakes occurred each month. Two different classes of  
 442 Magnitude have been created: MI < 2.0 (b), 2.0 < MI < 3.0 (c). No events of MI > 3.0 occurred in the area between 1986 and 2017.

| Year      | Brief description of the event  |
|-----------|---|
| 991       | Seasonal pool fed by springs  |
| 1828      | Bursts of the springs water flow. Uprising of muddy waters and clays ( <i>Raffaelli, 1869; De Stefani, 1879</i> )           |
| 1843      | Bursts of the springs water flow. Uprising of muddy waters and clays ( <i>Raffaelli, 1869; De Stefani, 1879</i> )           |
| 1876      | Subsidence and fracturing ( <i>De Stefani, 1879</i> )   |
| 1877      | Subsidence and fracturing ( <i>De Stefani, 1879</i> )   |
| 1962      | Bursts of the spring water flow. Uprising of muddy waters and clays ( <i>Giovannetti, 1975</i> )                            |
| 1969      | Abrupt falling of the water level and fracturing along the shores. The lake almost disappeared ( <i>Giovannetti, 1975</i> ) |
| 1985      | Arising of muddy waters in a well   |
| 1996      | Abrupt fall of the water level and fracturing along the shores  |
| 2016-2017 | Subsidence and fracturing   |

443 *Table 1 – Description of the activity at Prà di Lama lake*